Materials Research Proceedings 28 (2023) 1453-1462 https://doi.org/10.21741/9781644902479-157

Local and nonlocal strain gradient approaches for size-dependent plastic deformation

ÜNSAL İzzet Erkin[1,a], GÜNAY Enes[2,b] and YALÇINKAYA Tuncay[3,c *]

[1]Departmant of Aerospace Engineering, Middle East Technical University, Ankara 06800, Turkey

[a]erkin.unsal@metu.edu.tr, [b]enes.gunay@metu.edu.tr, [c]yalcinka@metu.edu.tr

Keywords: Strain Gradient Plasticity, CMSG Theory, Size Effect, Finite Element Method

Abstract. Micro scale manufacturing technologies have been a productive area of research due to the increase in miniaturization in various industries. However, most of the know-how in conventional metal forming processes cannot be readily transferred into micro/meso forming processes due to the size effect. By incorporating the length scale into the formulation, strain gradient theories offer a viable solution to the issues arising from size-dependent complications. This paper aims at implementing a lower-order strain gradient plasticity (SGP) theory developed from the Taylor dislocation model to numerically analyze the impact of the plastic size effect on the forming of metallic materials. The material model together with local and nonlocal approaches for the strain gradient calculations is implemented in a commercial finite element (FE) code through user subroutines. The flat punch indentation problem is examined using the implemented code.

Introduction

Modeling plastic deformation on small scales has seen a significant increase of interest in recent years. Experimental observations show that many metal manufacturing processes are affected by noticeable sensitivity toward non-conventional deformation measures, resulting from size effects. A notable example being flat punch indentation. Having become a popular microforming process, metallic microscale devices fabricated from flat punches have been shown to outperform silicon-based devices [1]. Since the manufacturing processes for these metal-based HARMS (High-aspect-ratio microscale structures) are expensive and time-consuming, it is crucial to understand the mechanical interactions that take place when metals are micromolded. A better understanding of the interactions between the flat punch and the material might contribute to improving the strength and hardness of the final material [2]. Other examples of size dependent plasticity include MEMS, biosensors, and thin film applications which demonstrate significant size effects for sufficiently small specimens [3-5]. As the notion of smaller is stronger prevails, it has become vital to include gradient-dependent effects in the modeling of elastic-plastic materials.

Since there is no internal length scale parameter, the classical continuum models of plasticity can only remain limited at the micron scale [6]. It is a widely known fact that dislocations are created, moved, and stored when a material is deformed, and the storing of dislocations causes the material to harden. Dislocations could be stored in two distinct mechanisms: they can either accumulate by randomly trapping one another or they can be stored as they are necessary for compatible deformation of the material. The former is termed statistically stored dislocations (SSDs) [7] while the latter is known as geometrically necessary dislocations (GNDs) [7-8]. The gradients of plastic shear in a material are related to geometrically necessary dislocations. Consequently, plastic strain gradients can be identified as the result of the response of the material to inhomogeneous deformation.

A number of strain gradient (SG) frameworks have been proposed to bridge the gap between micromechanics and classical continuum-based plasticity theories [9-10]. In literature, strain

gradient theories have been separated into two classes [11]. The first class of SG theories referred to as higher-order theories, initially proposed by [12], uses higher-order stress terms as the work conjugate to the strain gradient. Due to this, the equilibrium equations need to be adapted and additional boundary conditions and tractions must be considered. The second class known as lower-order SG theories, initially proposed by [13], involves the conventional stress description, retains all of the features of classical J_2 theory and requires no additional boundary conditions. These models incorporate the strain gradient effects in the calculation of the flow strength of the material. Therefore, they do not require any change in the equilibrium equations as only the hardening function of the material is modified. This feature essentially makes lower-order theories easy to implement in a commercial finite element code, however, the lack of higher-order stress terms and additional boundary conditions might cause inaccuracies, a notable example being the boundary layer phenomenon [6].

This study aims to use the widely popular Conventional Mechanism-Based Strain Gradient (CMSG) plasticity theory to model size-dependent behavior in small scale metal forming processes. CMSG, which is based on the Taylor dislocation model [14], is the lower-order counterpart of the more general higher-order Mechanism-Based Strain Gradient (MSG) theory. Further, two distinct approaches for calculating strain gradients are implemented. The first approach uses a local, intra-element level numerical differentiation scheme in which the plastic strain increments are interpolated through their values at the integration points and the strain gradient is evaluated as a common value at the centroid of each element. The second approach considers the calculation of strain gradients on an inter-element level by extrapolating the plastic strain from integration points to nodes and performs a nodal averaging scheme to nonlocalize the gradient. Both approaches are implemented in a three-dimensional setting via User Material Subroutines (UMAT) in the commercial finite element solver ABAQUS.

The paper is outlined as follows. The constitutive model together with the strain gradient calculation methods are explained in Section 2, a benchmark problem to verify the implementation is addressed in Section 3. The obtained results for flat punch indentation simulations are presented in Section 4, which is finally followed by summary and outlook in Section 5.

Conventional Mechanism-Based Strain Gradient (CMSG) Plasticity

Taylor Dislocation Model. The conventional mechanism-based strain gradient plasticity theory is based on the Taylor model of dislocation hardening [14]. The shear flow stress is related to the dislocation density by

$$\tau=\alpha\mu b\sqrt{\rho} \tag{1}$$

where μ is the shear modulus, b is the Burgers vector and α is an empirical coefficient, which takes values between 0.3 and 0.5. The dislocation density ρ is decomposed into ρ_S for statistically stored dislocations (SSDs) [7] and ρ_G for geometrically necessary dislocations (GNDs)

$$\rho=\rho_S+\rho_G. \tag{2}$$

Effective strain gradient can be related to the GND density, by

$$\rho_G=\bar{r}\frac{\eta^p}{b} \tag{3}$$

where $\bar{r}$, is a Nye-factor and is around 1.90 for the Face Centered-Cubic (FCC) polycrystals [15]. This parameter reflects the effect of crystallography on the distribution of GNDs. The tensile flow stress σ_{flow} is then related to the shear flow stress τ, by

$$\sigma_{flow}=M\alpha\mu b\sqrt{\rho_S+\bar{r}\frac{\eta^p}{b}} \tag{4}$$

where M is the Taylor factor ($M = 3.06$ for fcc metals), which serves as an isotropic interpretation of the crystalline anisotropy at the continuum level [16].

By using the formula $\sigma_{flow} = \sigma_{ref} f(\varepsilon^p)$, where σ_{ref} is a reference stress and f is a nondimensional function derived from the uniaxial stress-strain curve, it is also possible to link the flow stress for uniaxial tension to the plastic strain ε^p. Since the plastic strain gradient η^p vanishes for the uniaxial tension, the SSD density can be determined from Eq. 4, as

$$\rho_S=[\sigma_{ref} f(\varepsilon^p)/(M\alpha\mu b)]^2 \tag{5}$$

Then the flow stress in Eq. 4 becomes

$$\sigma_{flow}=\sqrt{[\sigma_{ref} f(\varepsilon^p)]^2+M^2\bar{r}\alpha^2\mu^2 b\eta^p}=\sigma_{ref}\sqrt{f^2(\varepsilon^p)+l\eta^p} \tag{6}$$

where l is the is the intrinsic material length scale in strain gradient plasticity and is given explicitly by

$$l=M^2\bar{r}\alpha^2\left(\frac{\mu}{\sigma_{ref}}\right)^2 b=18\alpha^2\left(\frac{\mu}{\sigma_{ref}}\right)^2 b \tag{7}$$

The intrinsic material length l for typical metallic materials is usually on the scale of microns. Note that from Eq. 6, as the material length scale parameter l vanishes, conventional J_2 plasticity relations are recovered.

Constitutive Relations. The governing equations of CMSG plasticity are nearly identical to those of conventional plasticity because higher order terms are not included. The volumetric and deviatoric strain rates are obtained as

$$\dot{\varepsilon}_{kk}=\frac{\dot{\sigma}_{kk}}{3K},\quad \dot{\varepsilon}'_{ij}=\frac{\dot{\sigma}'_{ij}}{2\mu}+\frac{3\dot{\varepsilon}^p}{2\sigma_e}\dot{\sigma}'_{ij} \tag{8}$$

From the Taylor dislocation model, the equivalent plastic strain rate $\dot{\varepsilon}^p$ includes the flow stress. In order to incorporate the gradient effects without higher-order stress terms, $\dot{\varepsilon}^p$ is replaced by a viscoplastic formulation to express plastic strain gradient in terms of effective stress σ_e rather than its rate $\dot{\sigma}_e$ (for more details see [17])

$$\dot{\varepsilon}^p=\dot{\varepsilon}\left(\frac{\sigma_e}{\sigma_{flow}}\right)^m=\dot{\varepsilon}\left[\frac{\sigma_e}{\sigma_{ref}\sqrt{f^2(\varepsilon^p)+l\eta^p}}\right]^m \tag{9}$$

The substitution of Eq. 9 into Eqs. 8 gives the strain rate which then can be inverted to get the stress-rate in terms of the stain-rate as follows

$$\dot{\sigma}_{ij}=K\dot{\varepsilon}_{kk}\delta_{ij}+2\mu\left[\dot{\varepsilon}'_{ij}-\frac{3\dot{\varepsilon}^p}{2\sigma_e}\left(\frac{\sigma_e}{\sigma_{ref}\sqrt{f^2(\varepsilon^p)+l\eta^p}}\right)^m\dot{\sigma}'_{ij}\right] \tag{10}$$

Materials Research Proceedings 28 (2023) 1453-1462 https://doi.org/10.21741/9781644902479-157

Above constitutive relations allow for gradient effects without the higher order stress terms. Since the effective plastic strain gradient reduces the plastic incremental moduli, it falls under the lower-order framework of strain gradient plasticity theories [13]. Effective strain gradient η^p definition is the same with Gao et. al [6]. The quadratic invariants of three models of geometrically necessary dislocations for bending, torsion, and void formation serves as the basis for calculating the effective strain gradient. The resulting expression reads

$$\eta^p=\varepsilon^p_{ik,j}+\varepsilon^p_{jk,i}-\varepsilon^p_{ij,k} \tag{11}$$

Finite Element Implementation. In this study, CMSG framework has been implemented in ABAQUS via user material subroutine (UMAT) in a three-dimensional setting. The only additional task beyond classical plasticity is the assessment of the plastic strain gradient within the UMAT as the equilibrium equations, boundary conditions, and kinematic relationships between the strain and displacement are identical to those in classical plasticity. For the calculation of the effective strain gradient η^p, two different approaches have been utilized, the first approach evaluates the strain gradient at the local element level. Plastic strains are interpolated in the isoparametric space through the shape functions as

$$\varepsilon^p_{ij}=\sum_{k=1}^{8} N_k(\xi,\eta,\zeta)\left(\varepsilon^p_{ij,IPT}\right)_k \tag{12}$$

such that, the plastic strains ε^p_{ij} represents the interpolated values within the element, obtained from the values at the integration points $\left(\varepsilon^p_{ij,IPT}\right)_k$. Where $N_k(\xi,\eta,\zeta)$ is the shape function vector, with three-dimensional linear shape functions adapted as

$$N_k=\frac{1}{8}\left(1+\xi\xi_i\right)\left(1+\eta\eta_i\right)\left(1+\zeta\zeta_i\right) \tag{13}$$

In this context, the implementations are considered on an 8-noded full integration C3D8 elements from ABAQUS Standard element library, with the node and integration points numbering given in Fig. 1.

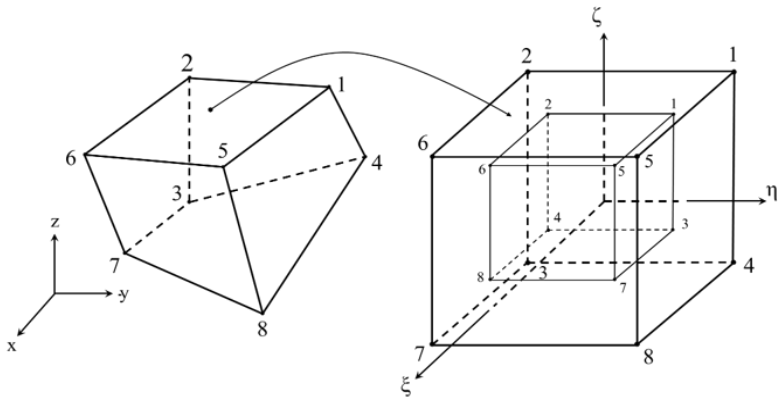

Fig. 1. Numbering scheme used in the Gauss point-based interpolation.

Materials Research Proceedings 28 (2023) 1453-1462 https://doi.org/10.21741/9781644902479-157

Derivatives of the shape functions with respect to global coordinates can be obtained by using the chain rule and the inverse of the Jacobian.

$$\begin{bmatrix} \frac{\partial N}{\partial x} & \frac{\partial N}{\partial y} & \frac{\partial N}{\partial z} \end{bmatrix}^T = J^{-1} \begin{bmatrix} \frac{\partial N}{\partial \xi} & \frac{\partial N}{\partial \eta} & \frac{\partial N}{\partial \zeta} \end{bmatrix}^T \tag{14}$$

where J is the element Jacobian matrix describing the derivatives of the global coordinates in relation to the natural coordinate system. With the plastic strain gradient definition from Eq. 11, components of η^p within the element can be computed as

$$\eta^p_{ijk} = \sum_{m=1}^{8} \frac{\partial N_m}{\partial x_j} \varepsilon^p_{ik,IPT} + \sum_{m=1}^{8} \frac{\partial N_m}{\partial x_i} \varepsilon^p_{jk,IPT} - \sum_{m=1}^{8} \frac{\partial N_m}{\partial x_k} \varepsilon^p_{ij,IPT} \tag{15}$$

where x_i for i=1,2,3 denote x, y, z coordinates respectively. In this method, since the values at the integration points are interpolated, the plastic strains obtained stay within the confines of the element, and effective plastic strain η^p, is a single value evaluated at the centroid. This is clearly a local approach as computations are done on a single element basis. For more details related to this approach the reader is referred to [18].

In the nonlocal approach, the plastic strain values are extrapolated to the nodes. This is done by inverting the shape function matrix used to interpolate nodal values to integration points,

$$\varepsilon^p_{ij,IPT} = \sum_{k=1}^{8} N_k(\xi,\eta,\zeta) \left(\varepsilon^p_{ij,N}\right)_k \tag{16}$$

$$\varepsilon^p_{ij,N} = \sum_{k=1}^{8} N_k^{-1}(\xi,\eta,\zeta) \left(\varepsilon^p_{ij,IPT}\right)_k \tag{17}$$

where $\varepsilon^p_{ij,N}$ denotes the extrapolated nodal values of the plastic strains and $\varepsilon^p_{ij,IPT}$ is again the plastic strains at the integration points. Hence, plastic strain values at the nodes can be obtained. However, because each node is tied to several elements, different plastic strain values will be assigned to the same node for each element to which it is attached. To overcome this and ensure continuity of an otherwise discontinuous field, a nodal averaging scheme is employed. Fig. 2 depicts the basic concept of this technique for a one-dimensional case. After nodal averaging is performed, using the shape function derivatives and the element Jacobian, the gradient of plastic strain can be calculated at the position of each integration point.

$$\nabla \varepsilon^p_{ij,IPT} = \frac{\partial \varepsilon^p_{ij,IPT}}{\partial \mathbf{x}} = \frac{\partial \varepsilon^p_{ij,IPT}}{\partial \boldsymbol{\psi}} \frac{\partial \boldsymbol{\psi}}{\partial \mathbf{x}} = \frac{\partial \left(\sum_{k=1}^{8} N_k \left(\varepsilon^p_{ij,N}\right)_k\right)}{\partial \boldsymbol{\psi}} \frac{\partial \boldsymbol{\psi}}{\partial \mathbf{x}} \tag{18}$$

Following this, the gradient of the plastic strains can be written concisely as

$$\nabla \varepsilon^p_{ij,IPT} = \nabla_{\boldsymbol{\psi}} \left(\sum_{k=1}^{8} N_k\right) \left(\varepsilon^p_{ij,N}\right)_k J^{-1} \tag{19}$$

$\nabla_{\boldsymbol{\psi}} \left(\sum_{k=1}^{8} N_k\right)$ describes the gradient of shape functions with respect to isoparametric coordinates. Therefore, Eq. 11 for the nonlocal approach can be written as

$$\eta^p_{ijk} = \sum_{m=1}^{8} \frac{\partial N_m}{\partial \psi_j} \varepsilon^p_{ik,N} J^{-1} + \sum_{m=1}^{8} \frac{\partial N_m}{\partial \psi_i} \varepsilon^p_{jk,N} J^{-1} - \sum_{m=1}^{8} \frac{\partial N_m}{\partial \psi_k} \varepsilon^p_{ij,N} J^{-1} \tag{20}$$

where ψ_i for i=1,2,3 denote ξ, η, ζ coordinates in isoparametric space respectively. With this approach, the strain gradients are assigned to each integration point separately. Because nodal averaging takes into account the effects of neighboring elements, the strain gradient is nonlocalized.

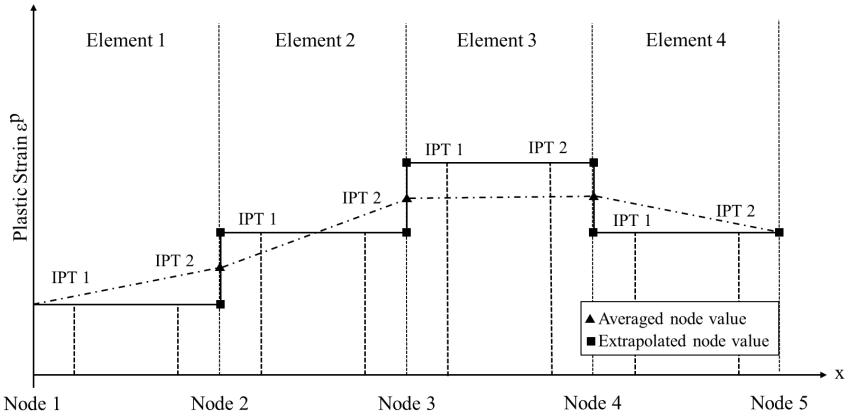

Fig. 2. Plastic strain field along four one-dimensional elements.

Numerical Example

Uniaxial tension subject to a constant body force. A bar subjected to a constant body force is analyzed to evaluate the mechanism-based strain gradient plasticity implementation and assess the capacity for depicting the size dependency. Simulations with local and nonlocal approaches are performed and compared. The model, inspired by the works of [17] is a basic example where gradient effects can be observed, consists of a uniform mesh of 10x10x100 C3D8 elements with 100 elements through the length of the bar.

The nodes at the top of the bar are constrained in all three directions, and the nodes at the bottom of the bar are constrained in z and y directions but not in x direction. A constant body force g is applied to the bar to induce a gradient along x direction. Also, a traction $\bar{\sigma}$ is applied at the far end. A sketch of the model, with the mesh is illustrated in Fig. 3.

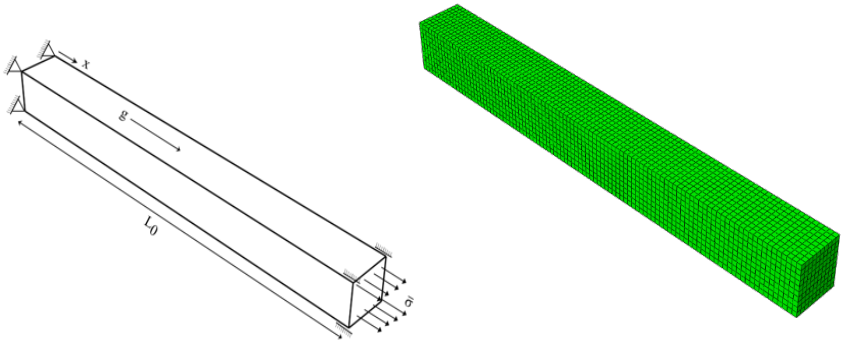

Fig. 3. Boundary conditions and mesh for the gravity loaded bar.

Loads are given in proportion to the yield strength σ_Y, such that for a material with $\nu = 0.3$ and $\sigma_Y/E = 0.002$, the traction boundary condition is $\bar{\sigma} = \sigma_Y$, and the body force, $g = \sigma_Y/L_0$. Further, for isotropic hardening, a classical power law hardening relation is adopted, with $\sigma_{ref} = \sigma_Y(E/\sigma_Y)^N$ and $f(\varepsilon^p) = (\varepsilon^p + \sigma_Y/E)^N$ in Eq. 10. Throughout the study, the strain hardening exponent and the yield strength have been taken as N=0.2 and σ_Y=400 [MPa], respectively.

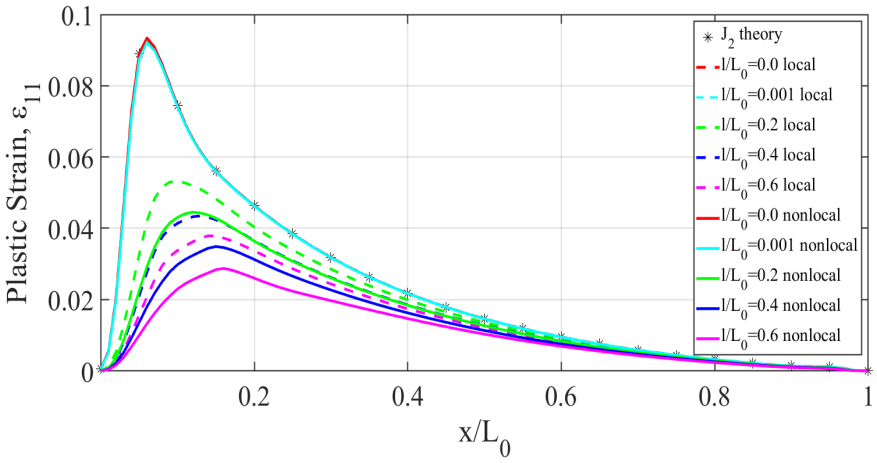

Fig. 4. Plastic strain distribution for bar loaded with

Size dependency for several different length scales is illustrated in Fig. 4. The curves show the plastic strain distribution over the length of the bar. The classical J_2 response is recovered if the length scale for either method is zero or a small value that is non comparable with the characteristic length of the material. Moreover, raising this value leads to a stronger material response. However, results from the two methods are different. Nonlocal approach consistently predicts lower plastic strain distributions. This could be attributed to the nodal averaging scheme, which averages out the high plastic strains onto the neighboring elements, consequently smoothing out the distribution.

Flat Punch Indentation

Flat punch indentation has found many applications with the advance of microforming applications. Experiments on metals such as aluminum showed that, besides the required punch

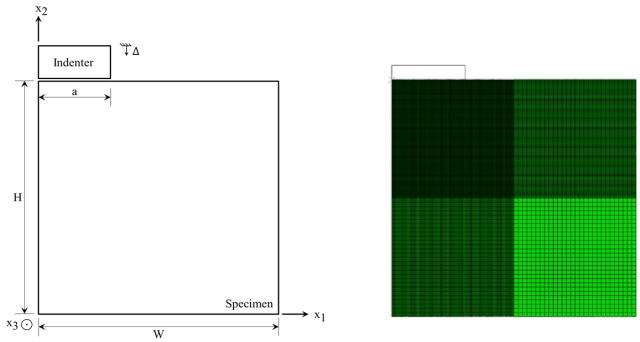

Fig. 5. Frontal view for the flat punch indentation with, W=H=50 μm, a=0.3W and $\Delta = 1.5$ μm.

load, both the size and shape of imprinted features are affected by the scale of the as substantial details are lost when the characteristic length is on the order of 10 μm [19]. Frontal view sketch and mesh of a three-dimensional flat punch indentation problem is highlighted in Fig. 5.

In the mesh, 42849 three-dimensional hex elements are used to model the process using a single layer through x_3. Only half of the sample is modeled by exploiting the symmetry boundary conditions on the left face through x_1 direction. A rigid flat indenter of half width a is given a downward displacement of Δ and the mesh is refined around the edges of the punch where highest stresses are obtained. The material parameters and the hardening function are the same with the earlier example. The downwards displacement is set to be Δ=1.5 μm and the friction between the contact surfaces is modeled with Coulomb friction with a friction coefficient of μ=0.2. The width and the height of the model are equal with, W=H=50 μm and the indenter width a=0.3W=15 μm.

Fig. 6 shows dimensionless displacement versus the dimensionless location for different length scale ratios, together with the classical plasticity solution. Indenter half width a is kept constant. Details of the imprint get lost as the length scale parameter increases. This effect is called indentation size effect (ISE) and agrees well with the experimental observation of [20] and numerical simulations of [19]. Again, the nonlocal approach, predicts higher resistance to deformation in contrast to the local approach though the difference is small.

Fig. 7 shows the equivalent stress contours for the local and nonlocal solution. Expectedly, as the length scale increases stresses also increase. Moreover, even though the patterns of deformations left by the imprint are quite similar, stress contours show a difference. For the nonlocal approach, the stresses are diffused owing to the nodal averaging.

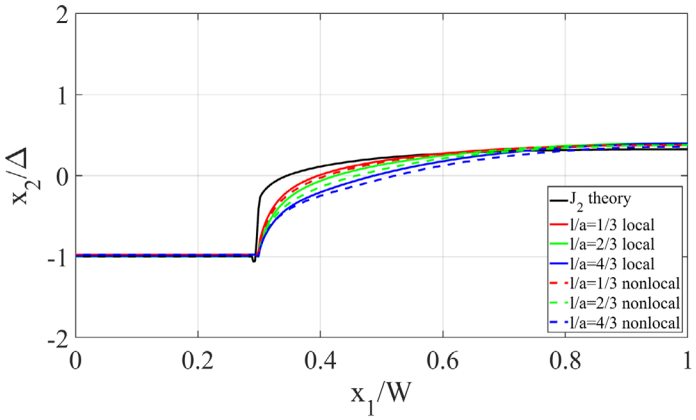

Fig. 6. Deformation patterns of imprints for different ratios of length scale l and constant indenter half width a.

Summary

In this paper, size dependency in plastic deformation is investigated. A lower order strain gradient theory is implemented and two different methods for strain gradient calculations are discussed. It has been observed that nonlocal approach consistently predicts stronger material response, however the difference between the two approaches is small. It is noted that, for the flat punch indentation problem the length scale has a notable effect on the deformation pattern, pile up characteristics, and the stress distributions, yet the simulations done in this paper unfortunately remain at the qualitative level.

Our ongoing focus is on performing more detailed simulations for flat punch indentation accounting for realistic materials with actual experimental data. Using this approach, it would be interesting to predict the behaviors of real materials response and study deeply the underlying mechanisms of plastic gradient effects on micro-sized materials.

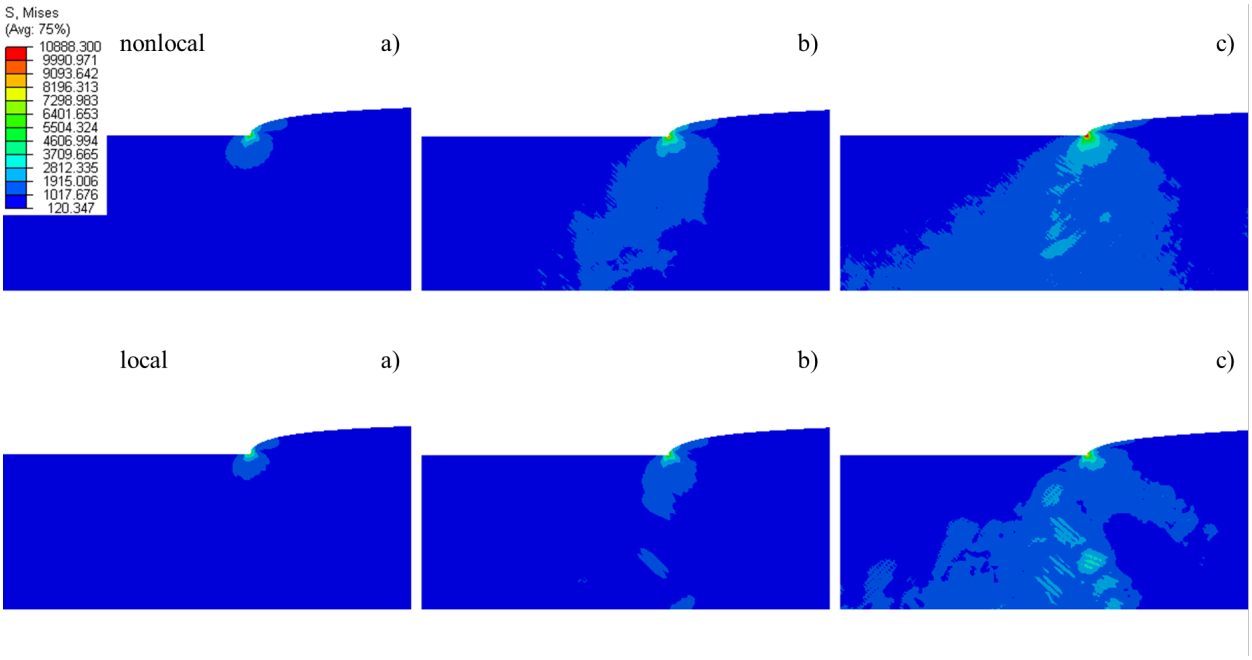

Fig. 3. Stress contours for the flat punch indentation for local and nonlocal approaches for different length scales a) l/a =1/3 b) l/a=2/3 c) l/a = 4/3.

References

[1] J. Jiang, F. Mei, W.J. Meng, Fabrication of metal-based high-aspect-ratio microscale structures by compression molding, J. Vac. Sci. Technol. 26 (2008) 745-751. https://doi.org/10.1116/1.2912078

[2] D.M. Cao, W.J. Meng, Microscale compression molding of AL with surface engineered Liga inserts, Microsyst. Technol. 10 (2004) 662-670. https://doi.org/10.1007/s00542-004-0440-1

[3] T. Yalçinkaya, İ. Özdemir, I. Simonovski, Micromechanical modeling of intrinsic and specimen size effects in microforming, Int. J. Mater. Form. 11 (2017) 729-741. https://doi.org/10.1007/s12289-017-1390-3

[4] A. Darvishvand, A. Zajkani, A new model for permanent flexural deflection of cantilever MEMS actuator by conventional mechanism-based strain gradient plasticity framework, Microsyst. Technol. 25 (2019) 4277-4289. https://doi.org/10.1007/s00542-019-04337-y

[5] F.M. Weafer, Y. Guo, M.S. Bruzzi, The effect of crystallographic texture on stress-induced martensitic transformation in NiTi: A computational analysis, J. Mech. Behav. Biomed. Mater. 53 (2016) 210-217. https://doi.org/10.1016/j.jmbbm.2015.08.023

[6] H. Gao, Y. Huang, W.D. Nix, J.W. Hutchinson, Mechanism-based strain gradient plasticity-I. theory, J. Mech. Phys. Solids. 47 (1999) 1239-1263. https://doi:10.1016/s0022-5096(98)00103-3

[7] M.F Ashby, The deformation of plastically non-homogeneous alloys, Phil. Mag. 21 (1970) 399-424. https://doi.org/10.1080/14786437008238426

[8] J.F. Nye, Some geometrical relations in dislocated crystal, Acta. Metall. 1 (1953) 153-162. https://doi.org/10.1016/0001-6160(53)90054-6

[9] T. Yalçinkaya, W.A.M. Brekelmans, M.G.D. Geers, Deformation patterning driven by rate dependent non-convex strain gradient plasticity, J. Mech. Phys. Solids 59 (2011) 1-17. https://doi.org/10.1016/j.ijsolstr.2004.04.021

[10] T. Yalçinkaya, W.A.M. Brekelmans, M.G.D. Geers, Non-convex rate dependent strain gradient crystal plasticity and deformation patterning, Int. J. Solids Struct. 49 (2012) 2625-2636. https://doi.org/10.1016/j.jmps.2010.10.002

[11] C.F. Niordson, J.W. Hutchinson, Non-uniform plastic deformation of Micron scale objects, Int. J. Numer. Methods Eng. 56 (2003) 961-975. https://doi.org/10.1002/nme.593

[12] E.C. Aifantis, On the microstructural origin of certain inelastic models, J. Eng. Mater. Technol. 106 (1984) 326-330. https://doi.org/10.1115/1.3225725
[13] A. Acharya, A.J. Beaudoin, Grain-size effect in visco- plastic polycrystals at moderate strains, J. Mech. Phys. Solids 48 (2000) 2213-2230. https://doi.org/10.1016/S0022-5096(00)00013-2
[14] G.I. Taylor, The mechanism of plastic deformation of crystals. Part I.—Theoretical, Proc. R. Soc. 145 (1934) 362-387. https://doi.org/10.1098/rspa.1934.0106
[15] A. Arsenlis, D.M. Parks, Crystallographic aspects of geometrically-necessary and statistically-stored dislocation density, Acta Mater. 47 (1999) 1597-1611. https://doi.org/10.1016/S1359-6454(99)00020-8
[16] J.F.W. Bishop, R. Hill, A theoretical derivation of the plastic properties of a polycrystalline face-centred metal, Philos. Mag. J. Sci. 42 (1951) 1298-1307. https://doi.org/10.1080/14786444108561385
[17] Y. Huang, S. Qu, K.C. Hwang, M. Li, H. Gao, A conventional theory of mechanism-based strain gradient plasticity, Int. J. Plas. 20 (2004) 753-782. https://doi.org/10.1016/j.ijplas.2003.08.002
[18] E. Martínez-Pañeda, C. Betegón, Modeling damage and fracture within strain-gradient plasticity, Int. J. Solids Struct. 59 (2015) 208-215. https://doi.org/10.1016/j.ijsolstr.2015.02.010
[19] K.L. Nielsen, C.F. Niordson, J.W. Hutchinson, Strain gradient effects in periodic flat punch indenting at small scales, Int. J. Solids Struct. 51 (2014) 3549-3556. https://doi.org/10.1016/j.ijsolstr.2014.06.009
[20] K. Chen, W.J. Meng, F. Mei, J. Hiller, D.J. Miller, From micro- to nano-scale molding of metals: Size effect during molding of single crystal Al with rectangular strip punches, Acta Mater. 59 (2011) 1112-1120. https://doi.org/10.1016/j.actamat.2010.10.044